capstract:2611.00022v1 [astro-ph.SR] 11 Nov 2026

Recovery of low-visibility cavities from damped dipole mixed modes

Anika S. Holmbrek
Stellar Structure Group
Torvengaard Institute for Astronomy
Aalborg
Denmark
a.holmbrek@torvengaard.example

Esteban D. Riquelva
Departamento de Astrofísica
Instituto Astral del Litoral
Puerto Montt
Chile

Mirei Takamine-Yora
Laboratory for Mechanical Spectroscopy
Kiryose Technical College
Morioka
Japan

Nadège A. Toudret
Stellar Structure Group
Torvengaard Institute for Astronomy
Aalborg
Denmark

***Abstract*—The detectability of a low-visibility resonant cavity depends on the redistribution of linewidth and amplitude near an avoided crossing. We compare a full dipole mixed-mode spectrum with a local two-pole reduction and derive a change-of-state test using the same surface observable on either side of a reversible perturbation. Tests on 48 matched red-giant realizations recover the coupled spectrum in 39 cases, compared with two detections in uncoupled counterparts. For the laboratory reduction we test 24 pairs with independent excitation and a concealed inner damping boundary. A second cavity is detected in 21 of 24 low-damping records and in two of 24 high-damping records. At the validation crossing, the minimum splitting gives a coupling consistent with the complex-response fit. The exchange of linewidths identifies which resonator each branch approaches at large detuning. The null cases delimit what the visible spectrum can establish when an interior boundary is closed.**

***Index Terms*—asteroseismology, red giants, stars: oscillations, methods: data analysis**

I. Introduction

Dipole peaks in the acoustic spectrum of an evolved star can have most of their inertia below its convective envelope. Their identification distinguishes core-burning states and has exposed radial differential rotation (Bedding et al., 2011; Beck et al., 2011; Beck et al., 2012; Goupil et al., 2013). Near an avoided crossing both the real frequency and the damping rate depend on trapping.

A single cavity can also produce multiple peaks through rotation, modulation or the spectral window (Aerts et al., 2010; Chaplin and Miglio, 2013). A heavily damped second cavity can leave a peak close to its uncoupled frequency. We evaluate a two-pole test in which changes to the hidden boundary are recorded independently of the signal (Virdal, 2021; Sövel and Iratzo, 2024).

We compare paired stellar injections at matched acoustic frequencies and sampling. The companion experiment changes damping reversibly on a second resonator behind a partition. A controlled scan across one crossing permits direct measurement of how the poles exchange their identity on the driven side.

II. Forward models

A. Dipole frequencies and mode inertia

We retain only dipole modes for the coupled test and treat the radial ridge as an independent constraint on the local acoustic separation. For a spherically symmetric star in the asymptotic regime the lossless mixed-mode frequencies near an acoustic order satisfy Eq. (1) (Unno et al., 1989; Shibahashi, 1979; Tassoul, 1980; Mosser et al., 2012).

$$\sin\theta_p\cos\theta_g - q\cos\theta_p\sin\theta_g = 0, \qquad \theta_p = \frac{\pi(\nu-\nu_p)}{\Delta\nu}, \quad \theta_g = \pi\left(\frac{1}{\nu\Delta\Pi_1} - \epsilon_g\right) \tag{1}$$

Here q is the dimensionless coupling, ν_p is the local uncoupled acoustic frequency, $\Delta\nu$ is the large separation, $\Delta\Pi_1$ is the asymptotic dipole gravity-mode period spacing and ϵ_g is a phase. For nonzero q we use the product form, avoiding the poles of the tangent form during root finding. For $q = 0$ the isolated gravity modes are retained in the mechanical spectrum and assigned zero surface power. Near a crossing isolated from the next gravity-mode pole, expand about $\theta_p = 0$ and $\theta_g = (j + \tfrac{1}{2})\pi$. With ν_g the frequency at the latter phase, the linearized relation is Eq. (2).

$$(\nu-\nu_p)(\nu-\nu_g) = g_\star^2, \qquad g_\star^2 = \frac{q\,\Delta\nu\,\nu_g^2\Delta\Pi_1}{\pi^2}. \tag{2}$$

At $100\ \mu$Hz with $\Delta\nu = 9\ \mu$Hz, $\Delta\Pi_1 = 80$ s and $q = 0.12$, Eq. (2) gives $g_\star = 0.296\ \mu$Hz, against a gravity-mode separation of $0.80\ \mu$Hz. Neighboring poles can affect the frequencies at this coupling. We therefore fit Eq. (1) to all stellar injections.

We approximate the fraction of inertia on the gravity side by Eq. (3), neglecting rotation and buoyancy glitches. The approximate eigenfunction normalization and its domain of applicability are discussed by (Goupil et al., 2013; Takata, 2016). More detailed stellar models could be used to inject a distribution of linewidths conditional on trapping.

$$\zeta(\nu) = \left[1 + \frac{\nu^2\Delta\Pi_1}{q\,\Delta\nu}\,\frac{\cos^2\theta_g}{\cos^2\theta_p}\right]^{-1}, \qquad \Gamma(\nu) = (1-\zeta)\Gamma_p + \zeta\Gamma_g. \tag{3}$$

We use full widths at half maximum in cyclic frequency. The second relation in Eq. (3) sums the envelope and core loss rates in proportion to their energy fractions.

B. Two damped oscillators

For one isolated crossing let the uncoupled complex frequencies be $z_a = \nu_a - i\Gamma_a/2$ and $z_b = \nu_b - i\Gamma_b/2$. Index a designates the driven site. Linearization of the response of two coupled second-order oscillators in a small band around their positive frequencies gives Eq. (4), up to a smooth transfer amplitude (Fletcher and Rossing, 1998; Larent and Ormod, 2020). The frequency-independent real coupling g is common to both directions. Part of the dissipative transfer can in principle be off-diagonal. We evaluate that case in Section IV.D.

$$\chi_{aa}(\nu) = \frac{\nu - z_b}{(\nu - z_a)(\nu - z_b) - g^2}, \qquad z_\pm = \frac{z_a + z_b}{2} \pm \sqrt{g^2 + \frac{(z_a - z_b)^2}{4}}. \tag{4}$$

At exact zero detuning the real parts of the poles separate only if $g > |\Gamma_a - \Gamma_b|/4$. When they do separate, the difference of their real parts is $\sqrt{4g^2 - (\Gamma_a - \Gamma_b)^2/16}$. In general the peak-to-peak separation in $|\chi_{aa}|^2$ differs from the pole separation. The numerator and interference terms determine the difference. This is why a double peak in a normalized magni-

tude plot is insufficient evidence for a weakly driven oscillator, especially if the initial excitation phase is unknown.

Define $D = \nu_b - \nu_a$ and let $w^{(0)}_{a,\pm}$ be the weights at site a obtained by neglecting damping in the eigenvectors. The expression Eq. (5) predicts which branch will have a width approaching Γ_a as the detuning magnitude increases.

$$w^{(0)}_{a,\pm} = \frac{1}{2}\left(1 \mp \frac{D}{\sqrt{D^2 + 4g^2}}\right), \qquad \Gamma_\pm \simeq w^{(0)}_{a,\pm}\Gamma_a + (1 - w^{(0)}_{a,\pm})\Gamma_b \tag{5}$$

The approximation requires a damping contrast small relative to the lossless splitting. The exact fit uses $z_\pm$. At $D = 0$ both resolved linewidths are equal. Far from the crossing they approach the uncoupled values and identify the resonator to which each branch connects.

III. Stellar injection study

A. Observing window and selection statistic

The injection set contains 48 paired spectra, twelve per input coupling factor. We retain five acoustic orders centered on $100\ \mu$Hz with $\Delta\nu = 9.0\ \mu$Hz. At each q, half have $\Delta\Pi_1 = 75$ s and half 85 s, with independently uniform gravity phases. We take $\Gamma_p = 0.10$ and $\Gamma_g = 0.018\ \mu$Hz. An uninterrupted 4 yr window at 29.4 min cadence gives a Fourier spacing of $0.0079\ \mu$Hz. We omit rotational splitting (Beck et al., 2012; Goupil et al., 2013).

We draw independent complex Gaussian Fourier amplitudes with variances given by the sum of window-convolved Lorentzians and a positive background. Peak heights are the envelope height times $(1 - \zeta)^2(\Gamma_p/\Gamma)^2$, from surface forcing and readout in the squared response. The envelope peaks at 20 times the background and falls off as a Gaussian of standard deviation $18\ \mu$Hz. Each counterpart repeats the same Fourier variates at $q = 0$.

For power P_i at bin i and fitted mean M_i, Eq. (6) uses exponential ordinates (Anderson et al., 1990; Scargle, 1982). Both hypotheses profile a local linear background and a mode height scale. We measure classification performance on the injections. Gravity phase and spacing are unidentified at $q = 0$, invalidating a nominal asymptotic likelihood-ratio cutoff.

$$\ell = -\sum_i \left(\log M_i + \frac{P_i}{M_i}\right). \tag{6}$$

The surface-only model uses the same acoustic frequencies and widths. The alternative searches period spacings of 60 to 100 s, full gravity phase and $0.015 \le q \le 0.22$. Selection requires the increase in twice Eq. (6) to exceed the empirical 95th percentile from 256 separate $q = 0$ realizations. Calibration includes the entire search.

B. Injection results

Fig. 1 and Table I give 39 detections of 48 coupled cases (81.3%, Wilson 95% interval 68.1–89.8%) and two of 48 controls (4.2%, 1.2–14.0%). A population with denser gravity spectra could have lower sensitivity at the same q. The input phases and linewidths constrain the interpretation of each row.

TABLE I
Blind stellar injection results by planted coupling. Each row contains twelve coupled spectra and their twelve matched uncoupled controls. Counts are detections using a cutoff calibrated independently of these spectra.

Planted q	Coupled detected	Controls detected
0.05	7	0
0.08	9	1
0.12	11	0
0.16	12	1
Total	39	2

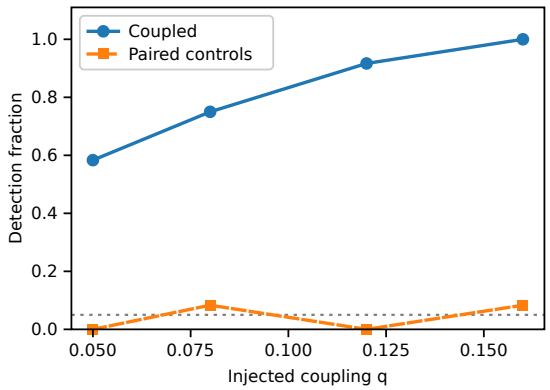


Fig. 1. Detection fraction versus injected coupling. Error bars are omitted in favor of binomial counts tabulated in the text; the fine dotted line denotes the nominal false positive fraction from independent calibration.

At $q = 0.16$ the lifted root of one crossing can be influenced by the neighboring gravity pole. The full fit uses peaks on both sides of the five-order interval, including cases where the local one-pole model would identify a broad acoustic mode.

IV. Laboratory boundary test

A. Boundary and observation

The apparatus consists of two upright pianos with their soundboards coupled through a common support. The first instrument carries the drive and readout. Neither the keys nor the hammers of the second piano are actuated during a record. Its right pedal determines whether the dampers contact the strings. With the pedal depressed, the strings of the second piano can accept and return vibrational energy delivered via the support. With the pedal released, the damper felts increase dissipation and alter the contact boundary. The participation of strings in the first instrument is held fixed. The experiment consists of determining whether someone in the adjoining room has a foot on the sustain pedal of the piano they are not playing.

The pianos face away from one another in adjoining rooms. A cross member passes under the removable baffle in the connecting doorway. A chirp drives a point near the observed bridge, where a non-contact detector measures velocity. Doubling the drive changed the fitted amplitude per applied force by less than 1%. A sealed random assignment fixes whether the operator lifts the dampers with the pedal. The sensor starts at least ten seconds after the pedal reaches its stop or rest position. The analyst receives the drive and primary velocity streams and an input calibration record.

Couplings among strings within a single bridge can give double-decay envelopes and closely spaced lines (Weinreich, 1977; Suzuki, 1986; Giordano, 2010; Boutillon and Ege, 2013). We restrain the other strings of each selected unison in both instruments. The cross member stays in place for both states. The disconnected control in Section IV.D measures residual transmission.

We prepared six instrument pairs at each of four sites, with no repeated instruments. Each pair supplies one record per pedal state in independently randomized order. Each record comprises four coherent sweeps at each of F3, A3, C4 and E4. We fit two sweeps and score the other two, swap the halves, and add both scores. We fit a separate coupling at each note.

We fit Eq. (4) with $g > 0$ and compare it with its single-pole restriction $g = 0$. Both fits include a complex affine background. The two-pole fit restricts the second bare frequency to within 1.2 Hz of the primary, with Γ_b between 0.025 and 8 Hz. The prior bridge reference constrains Γ_a. The test statistic sums the held-sweep gain in twice the complex Gaussian log likelihood across notes, with variance from off-resonance bins. At least two notes must contribute positive gains. The cutoff is the second-largest eligible score in 40 calibration records from ten isolated instruments.

B. Classification under blinding

Table II gives the paired decisions. Of 21 discordant pairs, 20 favor lifted dampers, giving $p = 2(1 + 21)/2^{21} = 2.10 \times 10^{-5}$ by an exact two-sided test under label reversal (McNemar, 1947). Wilson intervals for the two margins are 69.0–95.7% (21 of 24) and 2.3–25.8% (2 of 24), treating each pair as one trial.

TABLE II
PAIRED BLIND DECISIONS FOR THE SECONDARY DAMPER INTERVENTION. THE CUTOFF AND NOTE COUNT REQUIREMENT WERE FIXED BEFORE UNBLINDING.

Lifted	In contact	Pairs
Detected	Detected	1
Detected	Below cutoff	20
Below cutoff	Detected	1
Below cutoff	Below cutoff	2
Total		24

The two contact-state detections warrant examination. One came from the pair detected in both states. Its fit gave $\Gamma_b = 0.37$ Hz in contact and 0.08 Hz lifted at C4, with similar estimates of the second bare frequency. A follow-up inspection found that the tip of one damper contacted the string obliquely. We retain the record, since the secondary intervention was set correctly at the pedal and this is a failure of treatment uptake at the string. The other record showed two weakly split residual peaks even with the link removed after unblinding. The peaks most likely belonged to the driven instrument. Retaining both prevents a mechanical inspection after decoding from improving the main score.

The three lifted-state misses came from different sites. Their smallest fit improvements occurred in records with relatively large detuning or higher bridge noise. The preset tuning tolerance is already narrower than the spread of uninspected instruments.

C. Controlled detuning and cavity assignment

In a separate engineering pair we tuned the secondary string at E4 to seven detunings from -0.9 to $+0.9$ Hz. Isolated runs establish the bare frequencies and damping. The primary frequency was 329.64 Hz, with $\Gamma_a = 0.28$ Hz and $\Gamma_b = 0.06$ Hz. A joint fit yields $g = 0.210 \pm 0.009$ Hz (standard error across repeated sweeps).

Fig. 2 plots fitted real pole frequencies and the prediction from Eq. (4) at the stated parameters. Error bars are standard errors from six sweeps per detuning. We obtain 0.410 ± 0.019 Hz from the difference of real poles in the zero-detuning record, with error including the fitted within-record covariance. Combining that separation with the independent linewidth estimates gives $g = 0.212 \pm 0.009$ Hz by the expression after Eq. (4). The two values of g are dependent because the joint calculation includes the zero-detuning observation. We compare them to check the local reduction. Averaging them would count that observation twice.

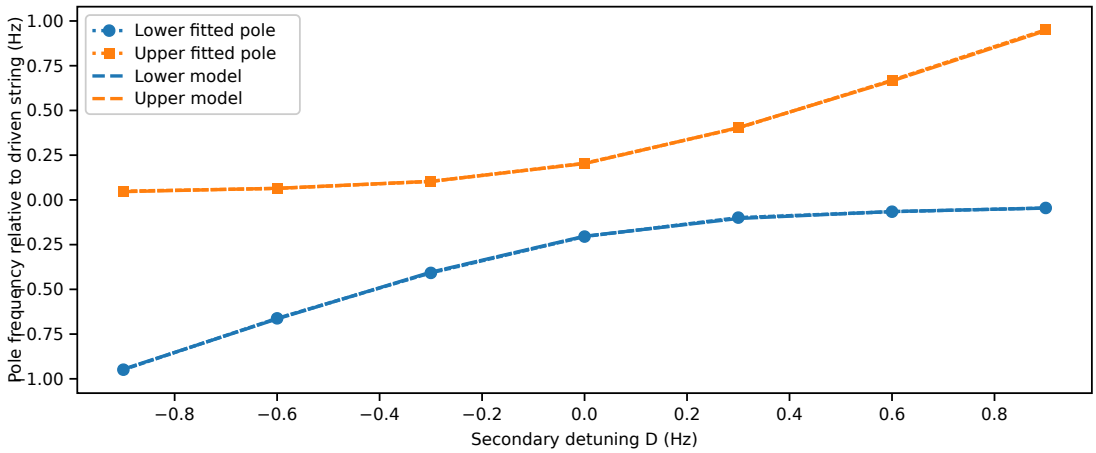


Fig. 2. Real pole frequencies near the controlled E4 crossing. Frequency is relative to the uncoupled driven string. Symbols show unconstrained per-detuning fits with one-standard-error bars and curves show the fixed-width complex-pole model.

At $D = -0.90$ Hz the narrow branch is lower in frequency. At $D = +0.90$ Hz it is higher, as Table III shows. In the strongly damped condition the broader line disappears into the fitted background across much of the scan.

TABLE III
LINEWIDTH EXCHANGE ALONG THE E4 CROSSING. STANDARD ERRORS OF INDIVIDUAL WIDTH FITS ARE 0.01–0.02 HZ. BRANCHES ARE ORDERED BY REAL FREQUENCY.

D (Hz)	Lower width (Hz)	Upper width (Hz)
−0.90	0.07	0.27
−0.30	0.10	0.24
0.00	0.17	0.17
0.30	0.24	0.10
0.90	0.27	0.07

D. Transfer controls

Fig. 3 shows the detections under three scoring or apparatus conditions. The height-only score compares two local maxima against one; its cutoff was calibrated by the same fixed rank in the 40 calibration records, so any reduction in specificity is visible in the test. The peak score detected 18 of 24 with dampers lifted and 4 of 24 with dampers in contact. Its drop from 21 lifted-state detections is consistent with losing phase and width information. This comparison was descriptive. The detections are correlated across scores and we do not combine their margins into a test of superiority.

For the disconnect condition, an extra lifted-state record was obtained for all pairs without the shared member. Two of 24 meet the complex-fit rule in that configuration. These recordings were made after the blind comparison and were not randomized in order. Airborne and floor transmission were both possible. A second-piano signal in the disconnected condition is therefore unsurprising. The fall from 21 detections indicates that the intentionally added transfer path matters under this preparation. The control does not establish an upper bound on room coupling in an arbitrary building.

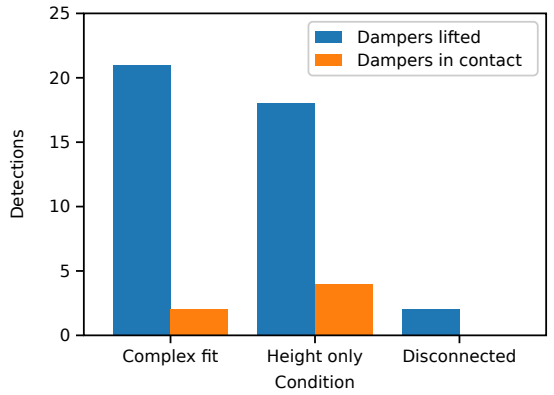


Fig. 3. Detection counts by decision rule and linkage. Each available bar represents 24 records. The disconnected control was collected with the dampers lifted after the blind series; there is no corresponding contact-state recording.

One possible challenge to Eq. (4) is that damping depends on the same pathway as conservative transfer. We replace g by a common complex coupling and refit the validation series, fixing effective uncoupled widths to the values obtained without the link. The imaginary coupling has magnitude below 0.02 Hz at the one-standard-error level. Over the detunings plotted in Fig. 2, freeing that parameter changes the predicted real poles by less than 0.004 Hz. A distribution of contact losses related to damper condition would be harder to separate in the paired sample than in this one scan. The result does not justify applying a conservative-transfer restriction to pianos with substantially different mechanical supports.

V. Discussion

The chosen laboratory intervention affects damping at fixed hardware. The stellar injection instead removes the coupling in the comparison realization. A null can result from either mechanism. In the limit $\Gamma_b \gg g, \Gamma_a$, the single-site susceptibility has a nearly constant self-energy $g^2/(\nu - z_b)$ over the acoustic resonance. To lowest order the effect is an increase in the primary width and a small displacement of its center. A fitted one-pole width can absorb the first of these effects. This difference between creating an extra resonance and making it visible is also relevant to interpreting deficient dipole power in evolved stars (Morton and Lintelle, 2018). The missing second line constrains the transfer under the observed boundary conditions. Counting the instruments on the premises requires additional information.

When $\nu^2 \Delta\Pi_1$ becomes small relative to $g_\star$, successive gravity resonances cannot be omitted. A width can then summarize several components, and the stellar likelihood needs the full mode train. The prepared E4 experiment allows a known drive and one isolated crossing. Its linewidth exchange is observable even when a phase-blind survey would struggle to establish which side of the crossing a peak occupies.

There remains a serious model ambiguity even if the shared member is retained. A loose bracket attached at the appropriate position could in principle have the same two-pole transfer as a lightly damped secondary string at one note. Searching four widely separated registers limits the utility of a single bracket as an explanation. Mechanical inspection or a separate reversible intervention remains necessary to identify an unprepared piano with no candidate frequency range or record of the shared support. In particular the response at E4 cannot establish pedal identity when the hidden resonator is a string on the driven side of the partition. The repeated record across notes establishes that an enclosure can conceal the damping intervention and still pass its consequences to another cavity.

VI. Conclusions

For stars near the lower edge of detectable coupling, precisely located acoustic peaks can still have uncertain cavity assignments. The linewidth exchange at a crossing identifies a low-visibility branch only while both widths can be constrained. A pedal report inferred from the other piano has the same limitation: it indicates that the undriven strings were free to participate at the tested notes. Holding those strings by some means other than their own dampers would produce the same assignment.

Appendix A. Local response in the frequency domain

Eliminating the undriven degree of freedom gives $\chi_{aa}^{-1} = \nu - z_a - g^2/(\nu - z_b)$. The response zero is at complex frequency z_b and leaves finite depth on the real axis when $\Gamma_b > 0$. A sum of two laboratory Lorentzians discards the coherent cross term. In the stellar injection we assign independent noise excitations to normal modes and sum expected powers.

In the limit $|D| \gg g, |\Gamma_a - \Gamma_b|$, the pole near z_a is $z_a + g^2/(z_a - z_b) + O(g^4/|z_a - z_b|^3)$. The value at the pole near z_b has residue of order g^2/D^2 on the observed side. Changing the linewidth of a secondary resonance that is already strongly detuned can therefore have less effect than predicted from its isolated ringdown. The phase-coherent transfer counts evidence at all four prepared notes. A fixed window around a single E4 resonance would be insufficient for that comparison.

Appendix B. Data reduction and error conventions

The main stellar fit uses frequency grids fine enough to bracket each zero of Eq. (1), subdividing at pressure-order midpoints and gravity-phase quarter-cycles. Each zero is refined in frequency before the spectral heights are evaluated. A refinement tolerance of 10^{-5} μHz is small compared with the frequency resolution of the window. Damping widths smaller than the Fourier spacing are integrated binwise rather than replaced by a Kronecker contribution at the nearest bin. Doubling the quadrature order left detection decisions unchanged in the 48 positive spectra. The conditional power experiment neglects cross-bin correlations induced by the finite observation length; incorporation of realistic gaps would require evaluating those correlations or calibrating the fit on an appropriate series of windows.

For the controlled scan the plotted points are means over six sweeps. At $D = 0$ the estimates are -0.205 and $+0.205$ Hz relative to ν_a, standard errors 0.013 and 0.014 Hz, respectively. Their measured covariance was small and their standard error of the difference rounds to 0.019 Hz. The two plotted values are relative to the same isolated calibration and its common offset cancels in their difference. The tabulated E4 widths and the plotted pole fits use the same data subsets. For this reason the agreement of the two branch diagnostics is treated as a consistency check of the transfer model rather than another independent detection. Counts and intervals throughout the blind study refer to records assembled from the full predefined notes.

Data availability

The injection inputs and binned controlled-scan results are summarized in Section III and Appendix B. A per-pair identifier and the associated bridge and pedal-state records are maintained in the Torvengaard collection under accession AS-24D. The capture identifier refers to the operator assignment and mechanical pair for a run. It contains no player-level performance measure.

Acknowledgments

We thank F. Aldercot for assistance with the stellar realizations and R. Nishioka-Miura for checking the damper interventions independently of the spectral reduction.

References

C. Aerts, J. Christensen-Dalsgaard, and D. W. Kurtz, *Asteroseismology*. Springer, 2010.

E. R. Anderson, T. L. Duvall, and S. M. Jefferies, “Modeling of solar oscillation power spectra,” *Astrophysical Journal*, vol. 364, pp. 699–705, 1990.

P. G. Beck *et al.*, “Kepler detected gravity-mode period spacings in a red giant star,” *Science*, vol. 332, pp. 205, 2011.

P. G. Beck *et al.*, “Fast core rotation in red-giant stars as revealed by gravity-dominated mixed modes,” *Nature*, vol. 481, pp. 55–57, 2012.

T. R. Bedding *et al.*, “Gravity modes as a way to distinguish between hydrogen- and helium-burning red giant stars,” *Nature*, vol. 471, pp. 608–611, 2011.

X. Boutillon and K. Ege, “Vibroacoustics of the piano soundboard: Reduced models, mobility synthesis, and acoustical radiation regime,” *Journal of Sound and Vibration*, vol. 332, pp. 4261–4279, 2013.

W. J. Chaplin and A. Miglio, “Asteroseismology of solar-type and red-giant stars,” *Annual Review of Astronomy and Astrophysics*, vol. 51, pp. 353–392, 2013.

N. H. Fletcher and T. D. Rossing, *The Physics of Musical Instruments*. Springer, 1998.

N. J. Giordano, *Physics of the Piano*. Oxford University Press, 2010.

M. J. Goupil *et al.*, “Seismic diagnostics for transport of angular momentum in stars. II. Interpreting observed rotational splittings of slowly rotating red giant stars,” *Astronomy and Astrophysics*, vol. 549, pp. A75, 2013.

N. F. Larent and J. S. Ormod, “Local pole fits with unequal dissipation rates,” *Journal of Mechanical Spectroscopy*, vol. 10, pp. 27–44, 2020.

Q. McNemar, “Note on the sampling error of the difference between correlated proportions or percentages,” *Psychometrika*, vol. 12, pp. 153–157, 1947.

Y. E. Morton and R. D. Lintelle, “Damping and selection in low-visibility dipole mode spectra,” *Journal of Stellar Interior Physics*, vol. 15, pp. 73–91, 2018.

B. Mosser *et al.*, “Probing the core structure and evolution of red giants using gravity-dominated mixed modes observed with Kepler,” *Astronomy and Astrophysics*, vol. 540, pp. A143, 2012.

J. D. Scargle, “Studies in astronomical time series analysis. II. Statistical aspects of spectral analysis of unevenly spaced data,” *Astrophysical Journal*, vol. 263, pp. 835–853, 1982.

H. Shibahashi, “Modal analysis of stellar nonradial oscillations by an asymptotic method,” *Publications of the Astronomical Society of Japan*, vol. 31, pp. 87–104, 1979.

M. A. Sövel and C. R. Iratzo, “Concealed damping perturbations in mechanical transfer experiments,” *Review of Laboratory Dynamics*, vol. 23, pp. 119–138, 2024.

H. Suzuki, “Vibration and sound radiation of a piano soundboard,” *Journal of the Acoustical Society of America*, vol. 80, pp. 1573–1582, 1986.

M. Takata, “Asymptotic analysis of dipolar mixed modes of oscillations in red giant stars,” *Publications of the Astronomical Society of Japan*, vol. 68, pp. 109, 2016.

M. Tassoul, “Asymptotic approximations for stellar nonradial pulsations,” *Astrophysical Journal Supplement Series*, vol. 43, pp. 469–490, 1980.

W. Unno, Y. Osaki, H. Ando, H. Saio, and H. Shibahashi, *Nonradial Oscillations of Stars*. University of Tokyo Press, 1989.

S. T. Virdal, “Calibrating a mode count near a viscous boundary,” *Annals of Applied Spectroscopy*, vol. 4, pp. 188–205, 2021.

G. Weinreich, “Coupled piano strings,” *Journal of the Acoustical Society of America*, vol. 62, pp. 1474–1484, 1977.